Gyrator-Capacitor Simulation Model of Nonlinear Magnetic Core*

Qianhong Chen[1], Ligang Xu[1], Xinbo Ruan[1], Siu Chung Wong[2], and Chi K. Tse[2]
[1]College of Automation Engineering, Nanjing University of Aeronautics & Astronautics, Nanjing 210016, China.
[2]Department of Electronic and Information Engineering, Hong Kong Polytechnic University, Hong Kong, China.

***Abstract*- The gyrator-capacitor model of the magnetic components has shown it's superiority in simulation for the electric and magnetic information integrity, convenience in the modeling and the mixed magnetic and electronic system simulation. This paper proposes an improved gyrator-capacitor core model, with a nonlinear resistor to simulate the hysteresis characteristic, with a nonlinear capacitor to simulate the core saturation. The model equation is presented in this paper as well as the parameter determination and optimization method. The simulation B-H curve comparing with that in datasheet proves the validity of the modeling method. The proposed simulation model is used in the system simulation of a 400kHz buck converter and a multi-output converter with the magnetic amplifier regulator. The simulation results are consistent with the experimental results or the principle analysis, verifying the effectiveness of the proposed core model.**

I. INTRODUCTION

Modeling and simulation play a great role in the development of the electronic/electrical product today, so as to meet the requirement of decreased time to market and the high cost of prototyping. Magnetic component is one of the key parts of the electronic/electrical system. Due to the difficulty in the observation of the magnetic field, modeling and simulation play an especially important role in magnetic-designing and optimizing, as well as the mixed magnetic and electronic system analysis including the static and dynamic performance.

Several models are available for magnetic component. The distributed field model normally relies on computation method such as finite-element-analysis, which will provide the best possible accuracy while requiring huge computing cost making it difficult to be applied in transient system simulation [1]. Jiles-Atherton model (JA model)[2]-[3] is other kind of precise core model, used in some commercial electrical circuit simulation software such as Saber. However, the parameters of JA-model is from the viewpoint of micro-magnetic-material which are not familiar for power electronics engineer and lost of close connection with the characteristic magnetic parameters in B-H curve. Due to the complexity, JA-model still has the non-convergence problem not fit for the mixed magnetic and electronic system transient simulation. In addition, it is not capable of delivering acceptable accuracy in certain circumstances [4], [5], because the models do not take into account core geometries [1]. Ref.[6] models a transformer with nonlinear core of hysteresis described by the continuous piecewise hyperbolic functions and loop-traversing algorithm. Despite of the complexity, the hysteresis modeling approach of [6] lacks of physical meaning. Besides, the proposed transformer models of [6] do not suit the magnetic components with complex structure such as integrated magnetics. Magnetic reluctance model [7]–[8] is widely used, based on magneto-motive force (mmf)-voltage, flux-current and reluctance-resistance analogies which lead to much confusion in energy relation[9]–[10]. The inductance-transformer equivalent electrical circuit [11] of the magnetic component derived from it's magnetic reluctance model is also normally used, having the modeling difficulty with non-planar magnetic structures, breaking the magnetic components down into an electrical macro-model only reflecting the information in electrical domain[9]-[10].Gyrator-Capacitor model (G-C model) of the magnetic component, using mmf-voltage, flux rate-current and permeance-capacitance analogies, has shown it's superiority such as the duality principle's perfection especially in energy[9]-[10], the integrity of the electric and magnetic information[9], [10], [12], the convenience in the modeling and the mixed magnetic and electronic system transient simulation[1], [9]-[10], [12], a better way in understanding and designing of magnetic components[9],[10], [13]. G-C model includes two parts: electrical circuit and magnetic circuit. In the magnetic circuit, the permeance of a magnetic core is analogous to a capacitor. A gyrator represents a winding, being an electrical-magnetic interface that links the electrical circuit and the magnetic circuit.

To ensure the simulation accuracy, the nonlinearities of the magnetic component, should be represented in the model. Since the elementary representation of the core's nonlinearities in G-C model including the core saturation and hysteresis, flux leakage, proximity loss have been presented in [12], this paper focuses on the improved G-C model of the nonlinear magnetic core with saturation and hysteresis and it's implementation in software. An improved G-C core model with a nonlinear resistor to simulate the hysteresis is proposed, eliminating the major B-H loop width changing problem in the current G-C core model. Both the functional representation of the model and the parameter determination approach are also given in detail. The presented G-C core model is implemented in MAST language of Saber software, whose model parameters can be calculated from the input core parameters and optimized automatically. The consistence of the simulated

*Project Supported by National Natural Science Foundation of China (50507009)

B-H curves and that provided in datasheets of several magnetic cores proves the validity of the modeling method. The proposed simulation model is used in the system simulation of a buck converter and a multi-output converter with the magnetic amplifier (mag-amp) regulator. The experimental results are consistent with the simulation results, verifying the effectiveness of the proposed core model.

II. Proposed Gyrator-capacitor Core Model

The improved G-C model for the inductor shown in Fig. 1(a), being taken as an example, is as shown in Fig.1(b). In the proposed model, a constant capacitor in series with a voltage controlled voltage source, equivalent to a nonlinear capacitor, is used to simulate the core saturation; a constant resistor in series with a voltage controlled current source, equivalent to a nonlinear resistor, is used to emulate the core hysteresis.

The function description of the voltage controlled voltage source satisfies,

$$\begin{cases} e(v_c) = |a \cdot v_c|^n \cdot sign(v_c) \\ sign(v_c) = \begin{cases} +1 & v_c > 0 \\ -1 & v_c < 0 \end{cases} \end{cases} \quad (1)$$

which is further simplified from that offered in [11].

Combining $\Lambda_{eff} \cdot d\left[v_c + e(v_c)\right]/dt = \dot{\phi}$ and (1) yields the equivalent nonlinear capacitance,

$$\Lambda_{eff} = \frac{\Lambda}{1 + a \cdot n |a \cdot v_c|^{n-1}} \quad (2)$$

From Fig.1(b), (1) and (2), it can be seen that when the voltage v_c across capacitor Λ, which is in proportion to the core flux, is much lower than the saturation point, $e(v_c)$ is small, resulting the increase of v_c with that of Ni and thus the equivalent capacitance is about Λ; When v_c is nearly the saturation point, $e(v_c)$ become larger with a rapid increase. Thus v_c increases little with the increase of Ni because most of Ni drops at $e(v_c)$, indicating that the core reaches saturation with the equivalent capacitance much less than Λ meaning low permeability.

The function description of the voltage controlled current source satisfies,

$$\begin{cases} i(v_r) = \left|\left(\frac{b \cdot v_r}{r}\right)^m\right| \cdot sign(v_r) \\ sign(v_r) = \begin{cases} +1 & v_r > 0 \\ -1 & v_r < 0 \end{cases} \end{cases} \quad (3)$$

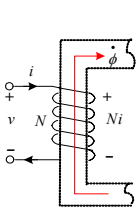

Fig.1(a) inductor

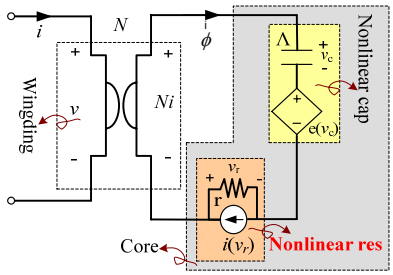

Fig.1(b)improved G-C model of the inductor

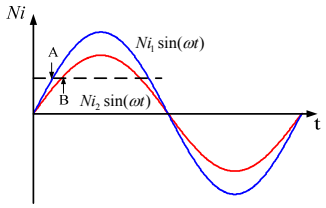

Fig.2 Sinusoidal exciting current with different amplitude

Combining $r_{eff}\dot{\phi} = v_r$ and (3) gives the equivalent nonlinear resistance,

$$r_{eff} = \frac{r}{1 + b\left|\left(\frac{bv_r}{r}\right)\right|^{m-1}} \quad (4)$$

Since v_r hinders the change of the magnetic flux, the B-H loop width will increase with the increase of v_r.

From Fig.1(b), (2) and (4), $\dot{\phi}$ is given by,

$$\frac{d(Ni)}{dt} = \frac{1}{\Lambda_{eff}}\dot{\phi} + \frac{d(r_{eff}\dot{\phi})}{dt} \quad (5)$$

When the core is not saturated, the effect of v_r on $\dot{\phi}$ is very small, and thus

$$\frac{d(Ni)}{dt} \approx \frac{1}{\Lambda_{eff}}\dot{\phi} \approx \frac{\dot{\phi}}{\Lambda} \quad (6)$$

If using linear resistor to model the core hysteresis as that in [11], when applying different exciting current with same frequency and different amplitude illustrated in Fig.2, to the G-C model, it can be find that the larger the amplitude, the larger the d(Ni)/dt and the corresponding flux rate at points with the same Ni value as A, B denoted in Fig.2, the larger the hysteresis loop width according to (6) even for major B-H loop. As for the proposed G-C model with nonlinear resistor in this paper, when v_r is low, $i(v_r)$ is small, the equivalent resistance is about r and the minor hysteresis loop width will increase with the increase of Ni; when v_r is large to operate nearly at the major B-H loop, $i(v_r)$ become larger with a rapid increase. Thus v_r increases little with the increase of Ni because most of current flows though $i(v_r)$, avoiding the major B-H loop width changing. The larger m, the littler change of the major loop width.

Without considering the core hysteresis, the analog relationship of the G-C model gives,

$$\begin{cases} B = v_c \Lambda / A_e \\ H = \left[v_c + (a \cdot v_c)^n \cdot sign(v_c)\right] / l_e \end{cases} \quad (7)$$

And thus the basic B-H curve of the core satisfies,

$$H = \left[\frac{BA_e}{\Lambda} + \left(\frac{aBA_e}{\Lambda}\right)^n \cdot sign(B)\right] / l_e \quad (8)$$

III. Parameter Determination Of The Model

A. *Input Model Parameters*

Input model parameters include two types: core material parameters and core geometry parameters. Core material parameters include B_{sat} (saturation flux density), H_{sat}

(saturation field intensity), B_r (remanence), H_c (coercive force), μ_r (relative permeability for the linear segment of the basic B-H curve), A_l (inductance per turn) and the basic B-H curve. Core geometry parameters include A_e (cross-section area), l_e (effective length of the field). The model parameters such as Λ, *a, n, r, b* and *m* are calculated based on the above-mentioned input model parameters.

It can be seen from the analysis in the last section that such parameters as Λ, *a* and *n* determine the basic B-H curve and the saturation characteristics of the core, which are called saturation parameters; based on the emulation of the basic B-H curve, such parameters as *r, b,* and *m* determine the hysteresis characteristics of the core, which are called hysteresis parameters.

B. Saturation parameters (Λ, a, n)

1) Define Λ.

The definition of the permeability gives,

$$\Lambda = (\mu_0 \mu_r A_e)/l_e \tag{9}$$

Thus Λ can be defined as A_l approximately according to the definition of A_l. To increase the accuracy, Λ should be defined according to the μ_r for the linear segment of the basic B-H curve since A_l is measured at very low excitation.

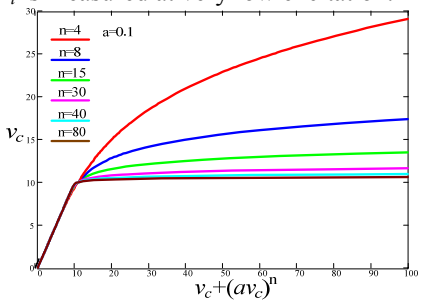

Fig.3 v_c versing $v_c+(a\cdot v_c)^n$ at different n

2)Decide *n*.

Seen from (7), the curve vc versing $v_c+(a\cdot v_c)^n$ reflects the characteristics of the basic B-H curve, which are shown in Fig.3 with different n and the same a (a=0.1). Comparing Fig.3 with the basic B-H curves of different magnetic material, it can be found that variable n mainly affects the dynamic permeability of the basic B-H curve, normally ranging between 3 and 7 for the powdered core, between 8 and 25 for the ferrites, and more than 30 for the core material with square B-H curve i.e. amorphous metal alloys. n can be decided based on the recommended experiential value.

3) Calculate *a*.

For non-square B-H curve core material, the saturation point satisfies,

$$V_{sat}+(aV_{sat})^n = H_{sat}le \tag{10}$$

Combining $B = v_c\Lambda / A_e$ with (10) yields,

$$\begin{cases} a = (\sqrt[n]{H_{sat}le - V_{sat}})/V_{sat} \\ V_{sat} = (B_{sat}Ae)/\Lambda \end{cases} \tag{11}$$

Since the *n* value is very large for the square B-H curve material, it can be estimated that the basic B-H curve transfers to saturation from linear state at the condition of $aV_{sat}=1$, thus,

$$a \approx 1/V_{sat} = \Lambda/(B_{sat}A_e) \tag{12}$$

Equation (11) and (12) disclose the relationship of n and a, ensuring the exact simulation of the saturation point.

4)Check *a* and *n*

Usually, the dynamic permeability of the saturation point is less than 10% of that in the linear segment of the basic B-H curve. That is

$$\Lambda_{eff\_sat}/\Lambda = 1/\left(1+a\cdot n\cdot\left|a\cdot V_{sat}\right|^{n-1}\right) < 0.1 \tag{13}$$

Parameters of *a* and *n* can be checked according to (13).

C. Hysteresis parameters (r, b, m)

1) Calculate r

It can be known from the definition of H_{sat} that when applying the excitation of $Ni=H_{sat}l_e sin\omega t$, the basic B-H curve of the core can be attained. When unsaturated, the core satisfies (6). And thus

$$\dot{\phi} \approx \Lambda\omega H_{sat}l_e\cos(\omega t) \tag{14}$$

When *Ni* is much lower than the saturation value, $\dot{\phi}$ is affected mainly by the changing rate of *Ni*. So, the $\dot{\phi}$ at B_r of the major B-H loop is approximate to that at origin of the basic B-H curve.

Combining $B = v_c\Lambda/A_e$, (14) and Fig.1(b) yields

$$\frac{B_r Ae}{\Lambda}+(a\cdot\frac{B_r Ae}{\Lambda})^n - r_{eff}\Lambda\omega H_{sat}l_e = 0 \tag{15}$$

Since the $\dot{\phi}$ at B_r point excited by the $H_{sat}l_e sin\omega t$ is not very large, r_{eff} decided by (15) is approximately to *r*,

$$r \approx \left[\frac{B_r A_e}{\Lambda}+\left(a\frac{B_r A_e}{\Lambda}\right)^n\right]\Big/\left(\Lambda\omega H_{sat}l_e\right) \tag{16}$$

For non-square B-H curve core material, the core is unsaturated at B_r. Hence the $\left(a\frac{B_r A_e}{\Lambda}\right)^n$ in (16) can be ignored leading to the calculation of *r* can be simplified further,

$$r \approx (B_r A_e)/\left(\Lambda^2\omega H_{sat}l_e\right) \tag{17}$$

2) Choose *m*

The larger *m*, the smaller the effect of the excitation amplitude on the major B-H loop width. m is normally larger than 10 to attain the good insensitivity of the major B-H loop width. If operation frequency is constant or changing a little, *m* is recommended to be chosen at 30 making the major B-H loop width insensitive to the excitation amplitude.

3) Calculate *b*

Since *m* is large enough, it can be known from (3) that:

when $bv_r/r>1$, $i(v_r)$ will take effect keeping the major B-H loop width unchanged; when $bv_r/r<1$, $i(v_r)$ will have little effect. So, H_c point satisfies $bv_r/r\approx 1$. For the H_c point, v_c and $e(v_c)$ equal to zero, and thus

$$v_r = H_c l_e \tag{18}$$

b can be calculated using the following equation,

$$b = 1.1r/(H_c l_e) \tag{19}$$

The coefficient for b in (19) is chosen as 1.1 because bv_r/r at H_c point is a bit larger than 1.

IV. Model Implementation and Parameter Optimization

The G-C model for the nonlinear core has been set up according to Fig.1(b), with the mast language in the Saber software environment. With the help of the program, the model parameters can be calculated and optimized automatically. And the engineering approximation and multi-solution problems of the model parameter determination method proposed in last section is solved at the same time. The implementation procedures are as follows,

Input the model parameters; The detailed parameters has been provided in section III.

2). Input the major B-H loop and the basic B-H curve of the core. The curve can be transferred to continuous data using the scanned data utility tool provided by Saber. And hence r can be obtained from the data transferred from the basic B-H curve.

3). Calculate Λ according to (8).

4) Optimize a, n adopting the method of least squares. The detailed implementing methods are as follows: Setting the calculating pace; ranging n between 2 to 40; calculating a according (11) and (12); selecting k points for B from the transferred basic B-H data linearly from $B_{sat}/3$ to B_{sat} and then calculating the corresponding $H_{s\text{-}i}$ (i=1,2,…,k); calculating the basic B-H curve fitting error ı with the least squares method according to (20) by comparing the calculated $H_{s\text{-}i}$ with the corresponding provided $H_{d\text{-}i}$; choosing the a, n with the minimum fitting error as the model parameter. Since the permeability around origin of the basic B-H curve is relative lower, the fitting error is calculated after $B_{sat}/3$ so as to ensure the fitting accuracy for the linear and saturation segments of the basic B-H curve. $B_{sat}/3$and k value can be regulated freely.

$$\varepsilon_1 = \sum_{i=1}^{k} (H_{d\_i} - H_{s\_i})^2 \qquad (20)$$

5) Choosing m=30, ranging r around the value calculated with (16), and then calculating b with (19). Applying the Ni exciting of $H_{sat}l_e \sin\omega t$ to get the simulated coercive force H_{cs} and saturation flux density B_{ss}, and then calculating the error,

$$\varepsilon_2 = (H_c - H_{cs})^2 + (B_{sat} - B_{ss})^2 \qquad (21)$$

choosing the r, b with the minimum fitting error as the model parameter.

V. Simulation Results

A. B-H Curve Simulation

To further testify the presented model and the parameter auto-calculation and optimization method, the inductors with EFD25 cores (using the geometry parameters defined by Philips) of 3 different material (lamination DWK85, ferrites NC2H of Nicera, ferrites 3H3 of Philips) are modeled and simulated using the circuit shown in Fig.1(b). The simulated major B-H loops are shown in Fig.4 (a) to (c) as well as the simulation condition. There is good consistency between the simulated major B-H loops and that provided in data book, indicating the validity of the proposed model and the parameter optimizing method. We also modeled the square B-H curve core of amorphous metal alloys Mp1305, whose simulated major B-H loop is as shown in Fig.4 (d). Because the major B-H loop is not provided in the data book, the comparison curve is not provided either. The key magnetic parameters of Mp1305 can be read out from Fig.4 (d) that B_{sat}=0.52T, H_c=11.87A/m and B_r=0.5T, which are very close to that offered in the data book.

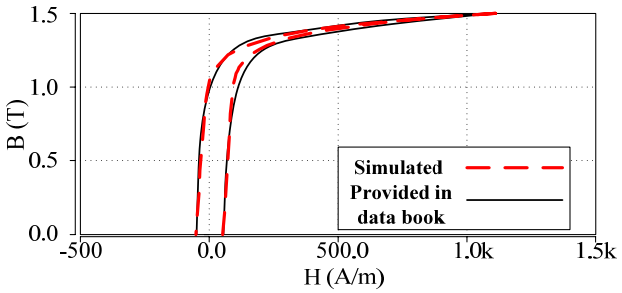

(a) Lamination DWK85:N=55, $i = 0.5\sin(2\pi \cdot 500 \cdot t)$

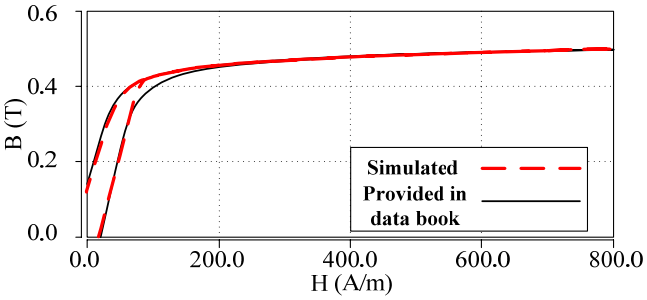

(b) Ferrites NC2H： N=55, $i = 0.5\sin(2\pi \cdot 100k \cdot t)$

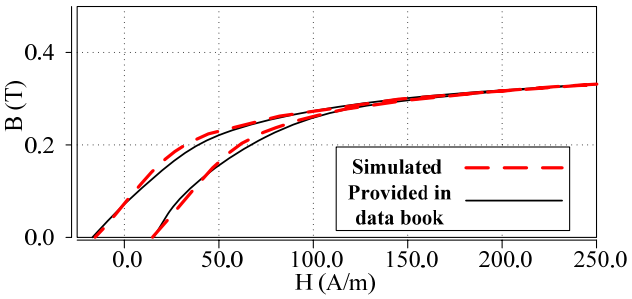

(c)Ferrites 3H3:N=55, $i = 0.5\sin(2\pi \cdot 100k \cdot t)$

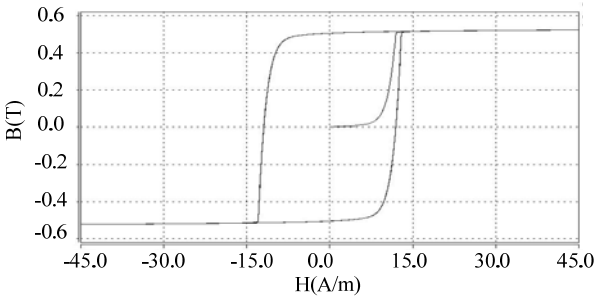

(d) Amorphous metal alloys Mp1305:N=9, $i = 0.5\sin(2\pi \cdot 100k \cdot t)$

Fig.4 Simulated major B-H loops of different magnetic material

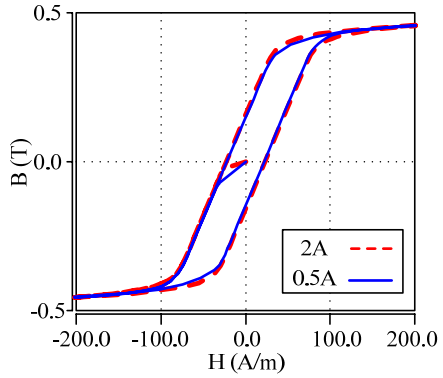

(a) Proposed G-C core model with nonlinear resistor

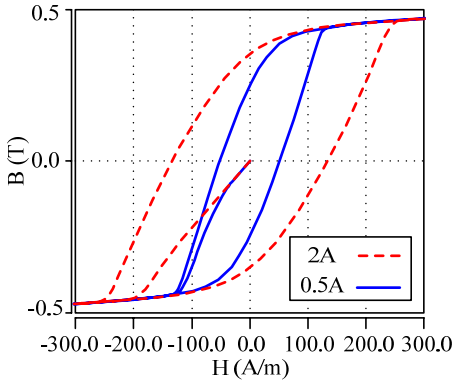

(b) G-C core model with linear resistor

Fig.5 Simulated major B-H loops at different amplitude of the exciting current with different core model

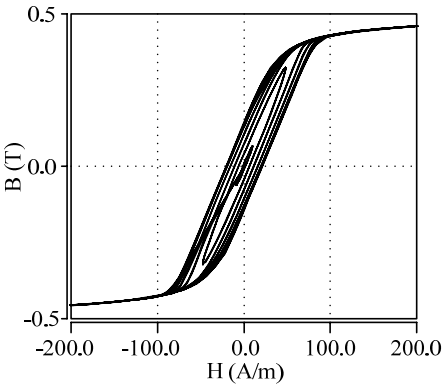

(a) At different amplitude

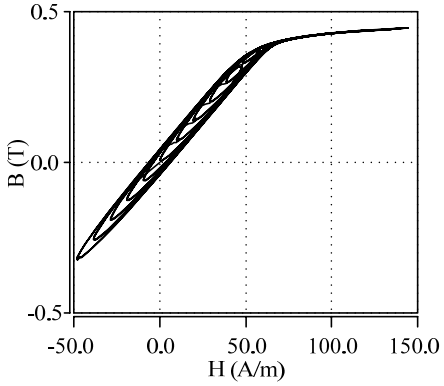

(b) At different DC bias

Fig.6 Simulated minor B-H loops at different amplitude or DC bias of the exciting current

,

For the same inductor referred to Fig. 4(b) (EFD25/NC2H ferrite core, N=55), using the G-C model with linear or nonlinear resistor, excited with $i = 0.5\sin(2\pi \cdot 100k \cdot t)$ or $i = 2\sin(2\pi \cdot 100k \cdot t)$, the major B-H loops are simulated and shown in Fig.5. Comparing Fig. 5(a) with Fig.5 (b), it can be seen that the major hysteresis loop width keeps unchanged using the proposed nonlinear resistor model while that will increase with the increase of magnetizing current amplitude using linear resistor core model. Fig6 also gives the simulated minor BH loops at different DC bias or amplitude of the exciting current.

B. Mixed Magnetic and Electronic System Simulation

A 24V input/12V, 1A output buck converter operating at 400*k*Hz, as Fig.7 shows, is simulated with the presented G-C inductor model. The inductor is fabricated with Nicera FEI-22 core of NC2H with the inductance of 8uH, whose detailed parameters are shown in Tab.I. Considering the gap of the inductor, a gap permeability Λ_{gap} should be in series with Λ in the G-C model[9]-[11]. The system simulated results are as shown in Fig.8. The current inductor has a step change in the switching transition. Combining the simulated inductor current waveform and it's operation B-H loop, it can be fund that, there is different Ni having the same B value with respect to different current changing direction leading to the current step change. That is caused by the core hysteresis. Fig.9 gives the measured inductor current waveform at full load. The simulated inductor waveform agrees well with the experimental results with a step change of about 0.25A in switching transition.

A 200V to 375V input, 5V/30A, 3.3V/14A output converter is also simulated with the proposed G-C model. The simulation circuit is as shown in Fig.10, where the 3.3 v output is implemented with mag-amp using the core of amorphous Mp1305, whose simulated major B-H loop has been presented in Fig.4(d). The static and dynamic simulated waveforms are as shown in Fig.11. It can be seen that the mag-amp core is positive saturated every perioid in steady state, consisting with the theoretical analysis. The simulation practice and results testify the applicability of the presented G-C core model in mixed magnetic and electronic system simulation.

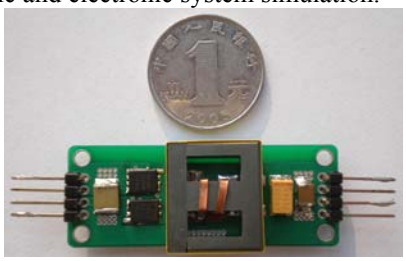

Fig.7 Prototype photo of the buck converter

Tab.1 Inductor parameters and it's model parameters

AL (uH)	Ae (mm2)	le (mm)	N	Bsat (T)	Hsat (A/m)	Br (T)
2.5	41.4	39.5	2	0.5	800	0.14
Λ (uH)	Λgap (uH)	n	a	r (Ω)	m	b
7.1	2.74	19	0.409	0.059	30	0.039

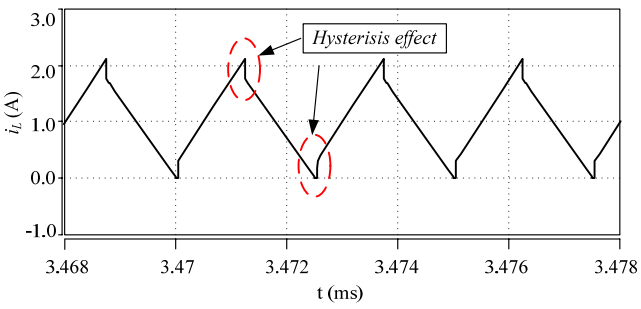

(a) Simulated inductor current waveform

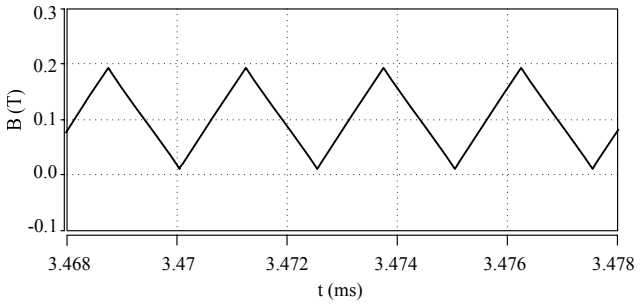

(b) Simulated inductor flux density waveform

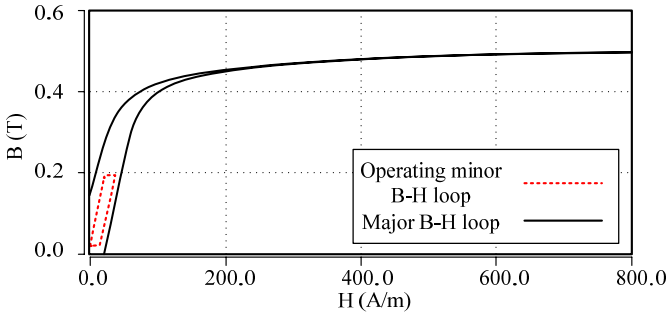

(c) Simulated operating minor loop

Fig.8 System simulation results of the buck converter at full load

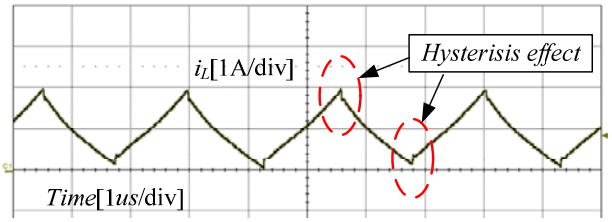

Fig.9 Measured inductor current waveform at full load

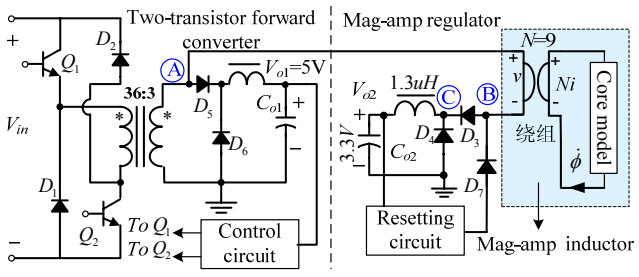

Fig.10 Simulation circuit sketch of the two output converter with mag-amp post regulator

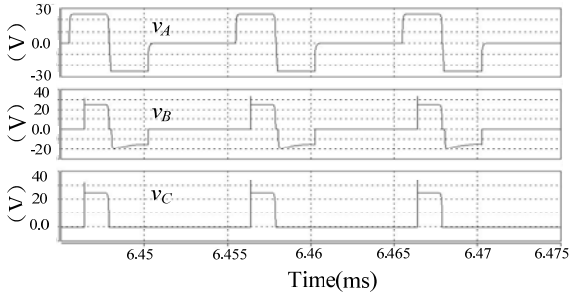

(a) Simulated operation waveforms

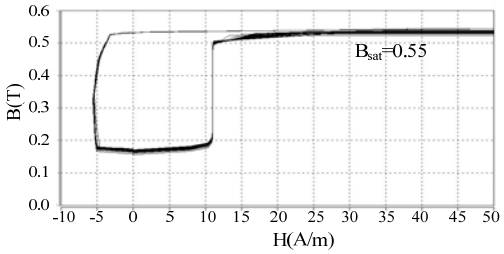

(b) Simulated operation B-H loop

Fig.11 Static simulation results at 200V input full load ouput

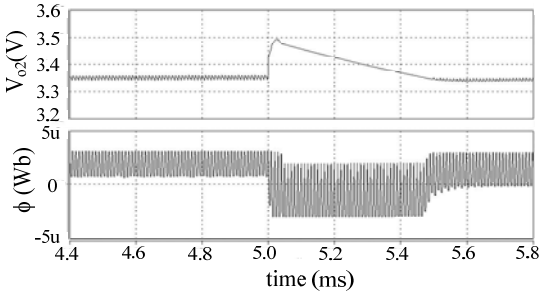

(a) Simulated dynamic waveforms

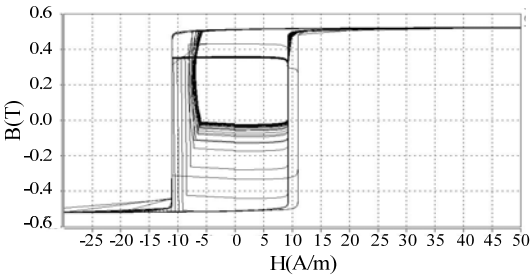

(b) Simulated operation minor B-H loops

Fig.12 Dynamic simulation results at 200V input and step down load change of 3.3V

VI. Conclusions

An improved G-C core model with better accuracy is proposed in this paper, with a nonlinear resistor to simulate the hysteresis characteristics eliminating the major B-H loop width changing problem, with a nonlinear capacitor to simulate the nonlinear permeability. The model equation is presented in this paper as well as the detailed parameter determination methods. The parameter automatic calculation and optimization methods in the Saber software environment are also offered. The simulation results verify the effectiveness of the proposed core model. The consistence of the simulated B-H curves and that provided in datasheets of several magnetic

cores proves the validity of the modeling method. The proposed simulation model is used in the system simulation of a buck converter and a multi-output converter with the magnetic amplifier (mag-amp) regulator. The experimental results are consistent with the simulation results, verifying the effectiveness of the proposed core model.

REFERENCES

[1] A.D.Brown, J. N Ross, K.G.Nichols. Time-domain simulation of mixed nonlinear magnetic and electronic systems[J]. IEEE Trans. on Mag 2001, 37(1): 522~532.

[2] P. R. Wilson, J. N. Ross, A. D. Brown. Optimizing the Jiles-atherton model of hysteresis by a genetic algorithm[J]. IEEE Trans. on Mag 2001, 37(2): 989-993.

[3] M. C. Willimas, R. S. Vogelsong, K. S. .Kundert. Simulation and Modeling of Nonlinear Magnetics[C]. IEEE ISCAS, 1995, 736~739

[4] D. A. G. Pedder, A. D. Brown, and J. A. Skinner. A contactless electrical energy transmission system[J]. IEEE Trans. on IE 1999, 46(1): 23~30.

[5] S. C.Wong and A. D. Brown. Analysis, modeling and simulation of series-parallel resonant converter circuits[J]. IEEE Trans. on PE 1995, 10(5):605–614.

[6] G.W. Ludwig, S. El-Hamamsy. Coupled inductance and reluctance models of magnetic components[J]. IEEE Trans. on PE 1991, 6(2):240~250.

[7] A.F. Witulski. Modeling and design of transformers and coupled inductors[C]. IEEE APEC, 1993, 589~595.

[8] R. Severns and E. Bloom, Modern DC/DC Switchmode Power Converter Circuits. New York: Van Nostrand Reinhold Company, Dec. 1985.

[9] D.C. Hamill. Lumped equivalent circuits of magnetic components: the gyrator-capacitor approach. IEEE Trans. on PE 1993, 8(2): 97~103.

[10] D.C. Hamill, Gyrator-Capacitor Modeling: A better Way of Understanding Magnetic Components[C]. IEEE APEC, 1994, 326~332.

[11] M. Eaton, Shoremine. Adding Flux Paths to SPICE's Analytical Capability Improves the Ease and Accuracy of Simulating Power Circuits[C]. IEEE APEC, 1998, 386~392

[12] L. Yan, B. Lehman. A Capacitor Modeling Method for Integrated Magnetic Components in DC/DC Converters[J]. IEEE Trans. on PE 2005, 20(5):987-996.

[13] D. K. Cheng, L.Wong, Y. S. Lee. Design, modeling, and analysis of integrated magnetics for power converters[C]. IEEE PESC, 2000, 320~325.

[14] P. G. Blanken. A lumped winding model for use in transformer models for circuit simulation[J]. IEEE Trans. on PE 2001, 16(3):445–460.

[15] Chen Qianhong,Ruan Xinbo,Yan Yangguang. Integrated magnetics technology and its application in power supply[J]. Transactions of China Electrotechnical Society,2004, 19（3）:1-8.

[16] L.P. Wong, Y.S Lee, D.K. Cheng. A New Approach to the Analysis and Design of Interated Magnetics. IEEE PESC, 2001:1196-1202.

[17] Zhaoxiuke. Practical technique data book of power supply -Magnetic components. Shenyang: Liaoning publishing house, Aug. 2002.